Journal of Building Engineering 98 (2024) 111110

Contents lists available at ScienceDirect

Journal of Building Engineering

journal homepage: www.elsevier.com/locate/jobe

Mass Timber Buildings: The associated risks of rainwater exposure during construction in the Portuguese climate

Daniel F. Lima [a,*], Sónia Duarte [b], Jorge M. Branco [a], Lina Nunes [b,c,1]

[a] ISISE, University of Minho, Campus de Azurém, 4800-058, Guimarães, Portugal
[b] National Laboratory for Civil Engineering, 1700-066, Lisbon, Portugal
[c] CE3c—Centre for Ecology, Evolution and Environmental Changes, Azorean Biodiversity Group, CHANGE – Global Change and Sustainability Institute, University of Azores, 9700-042, Azores, Portugal

ARTICLE INFO

Keywords:
Cross laminated timber
Climate exposure
Moisture content
Degradation risk
Scheffer climate index

ABSTRACT

The increase in the number and complexity of wooden buildings creates a series of challenges, like moisture control and management during the construction phase. The risks associated with the direct exposure of timber elements to rain during construction depend on the severity of the climate and the specific details of each project and therefore must be analysed locally. In this context, the results of 16 weeks of moisture content monitorization of Cross Laminated Timber (CLT) floor-wall connection specimens exposed to the outdoors are presented and evaluated. The monitorization demonstrated that end-grain surfaces are the most sensitive to the action and movement of water in CLT and within a few days of exposure to rain reached alarming moisture content (MC>30 %), with water entrapment at the interface between elements, preventing drying in a reasonable time for construction workflow (MC>30 % after 39 days of drying). On the other hand, zones with faster drying exhibited severe physical damage such as delamination and cracks. Additionally, the study evaluates the feasibility of using satellite-obtained meteorological data to develop a degradation risk map (Scheffer Climate Index) for mainland Portugal. The high coefficient of determination ($R^2 \geq 0.81$) and model efficiency (EF ~ 0.80–0.90) demonstrate the reliability of the data. Finally, two degradation risk maps for mainland Portugal are presented.

1. Introduction

Wood has a long-standing history as one of the oldest construction materials, valued for its abundance and favourable mechanical properties. As a natural, renewable material, it aligns well with efforts to reduce the ecological footprint of construction. Technological advancements in Engineered Wood Products (EWP), such as Glued Laminated Timber (GLT) and Cross-Laminated Timber (CLT), including improvements in production methods and connectors, have overcome previous limitations of wood as a structural material, extending its application to high-rise buildings [1–3]. Notably, on the publication date, the tallest timber building stands in Milwaukee (United States of America), boasting 25 floors and approximately 86.6 m in height [2,4,5].

EWP, like other wood-based products, are susceptible to biological (fungi, insects), physical, and chemical degradation. Fungal

* Corresponding author.
E-mail addresses: daniel.asmf.lima@gmail.com (D.F. Lima), sduarte@lnec.pt (S. Duarte), jbranco@civil.uminho.pt (J.M. Branco), linanunes@lnec.pt (L. Nunes).
[1] Lina Nunes (†) - deceased author.

https://doi.org/10.1016/j.jobe.2024.111110
Received 1 July 2024; Received in revised form 10 October 2024; Accepted 19 October 2024
Available online 20 October 2024

degradation, for instance, can diminish the aesthetic value of wood, impact indoor air quality, and, in severe cases, compromise its structural integrity, posing risks to the health and safety of occupants, increasing repair/maintenance costs, and reducing the service life of the building [6,7]. Despite its status as one of the forest-origin products with the highest added value, the durability of EWPs in diverse climates remains uncertain, largely due to their predominant use in central and northern Europe, where cold winters diminish the presence and activity of biotic agents of wood degradation [8,9].

Additionally, cyclic changes in temperature, relative humidity and exposure to rain lead to moisture content (MC) variations that can subsequently cause internal moisture-induced stresses capable of compromising the physical integrity of EWP with drying cracks, delamination, and excessive warping [10]. Therefore, the degradation process of wood is intricately linked to environmental conditions (air relative humidity, temperature, solar exposure, among others), the wood species, and its MC [6].

In this context, moisture is a key factor regarding mass timber durability, and many researchers are focusing their attention on understanding the moisture dynamics of emerging EWP to manage moisture-related damages [11–20]. To consider the building service life during all phases, including the construction phase, is fundamental, as a longer service life implies lower overall costs and enhanced environmental performance [11,21].

Hence, effective moisture management strategies must be incorporated across all phases, encompassing transportation, material storage, and construction processes. This represents a significant challenge for constructors, given that massive timber elements, such as CLT, exhibit non-uniform wetting patterns owing to the inherent anisotropy of wood coupled with the crossed laminations characteristic of CLT. Moreover, these elements tend to dry at a slower pace compared to traditional timber elements. This slower drying process can form moisture-trapping areas, thus accentuating the relevance of meticulous design detailing [11,22,23].

Thus, current European standards limit the use of CLT, one of the most used EWP for structural applications, to service classes 1 and 2 [2,24,25], in other words, without direct exposure to climate. Glulam, another widely used EWP in structures, does not have this specific limitation in the standards. However, it is still predominantly used in service classes 1 and 2 due to the low natural durability of the species used in Glulam production. In this context, performance-enhancing techniques for the materials used in EWPs can be applied, such as charring the surfaces exposed to the exterior. However, modifying the material performance can be financially and energy costly, in addition to altering the wood aesthetics and mechanical properties [26,27].

For a more sustainable alternative, the use of durable natural materials, like durable wood species, on the surfaces exposed to the exterior could be considered. One option that is gaining attention is the use of bamboo-based products. With advancements in flattening techniques, bamboo has overcome previous material limitations, making it more widely used in the construction sector in countries where bamboo is naturally abundant, such as China [28–30]. However, the most common practice nowadays is to apply CLT and Glulam without any surface performance enhancement, with cladding systems only being installed after the structural assembly, leaving the material exposed for most of the construction phase.

Despite the rapid assembly and shortened construction times associated with Mass Timber Buildings (MTB), the increasing complexity and height of new structures and the lack of experience among constructors can lead to a longer environmental exposure time during construction [11,31]. Additionally, the costs associated with ensuring watertight encapsulation of CLT at the factory are often considered high, leading designers and contractors to forego this option.

The MC of CLT panels was monitored during the construction phase in six buildings in Estonia, and, in some cases, despite the reduced installation time of the panels, the exposure time was prolonged due to delays in the application of the panels' facade protection layers [18]. Additionally, it was found that the protective measures of the panels with foils or membranes proved ineffective, allowing water infiltration and hindering proper drying. Regarding the monitoring results, MC was reported to be frequently above critical levels after single rain events, indicating that construction speed alone is insufficient to prevent excessive humidification [18]. Similarly, Austigard & Mattson (2020) [32], in Norway, reported that insufficient protection during construction, or construction errors, led to excessive water infiltration and moulds in nine out of twelve case studies and decay fungi in six out of twelve case studies.

Conversely, Schmidt & Riggio (2019) [31], in Oregon (United States), reported that in most cases, the MC remained below 16 % for almost the entire construction period. However, they cautioned that precipitation during the construction period was low and the available drying time for the structure was high, which does not correspond to the reality of many constructions. Nevertheless, the authors observed that in specific points where water accumulation was favoured and drying impaired, such as connections between elements with high shading, MC reached critical levels and even led to moisture entrapment in the interior layers of the elements [31]. This finding aligns with the results of both the monitoring and tests conducted by Kalbe et al. (2022) [18], where it was identified that the connection zone between a wall and floor panel represents a critical area, allowing the infiltration of large amounts of water through the end grain face and hindering drying due to lack of ventilation and shading caused by the interface between the two elements, an effect also reported by other authors [33].

The effects of built-in moisture on the structural performance of connections in EWP have being investigated recently but remain somewhat unknown. Yermán et al. (2021) [34] reported a loss of up to 70 % in nail withdrawal resistance after wetting and drying cycles. Conversely, Bora et al. (2022) [14] observed an increase in peak resistance in angle bracket connections following simulated rain exposure, with no significant changes in stiffness or energy dissipation. Meanwhile, Udele et al. (2023) [13] reported that aggressive drying induced angle bracket connections to fail more brittlely. It is worth noting that the mentioned studies focus on the short-term effects of humidification, while long-term, such as biological degradation, still face limitations in testing methods [35]. Furthermore, changes in MC alter EWP physical and mechanical properties, increasing density and reducing strength and stiffness, potentially affecting the dynamic behaviour of the building. However, the dynamic behaviour of new MTB is a subject that involves multiple variables, and the role of variations in MC and environmental exposure conditions still needs to be further studied [36–38].

The risks associated with exposure to rain of EWP should be analysed locally since it is directly related to the local climate. Schmidt & Riggio (2019) [31] emphasize the responsibility of decision-makers, such as designers and contractors, when planning the

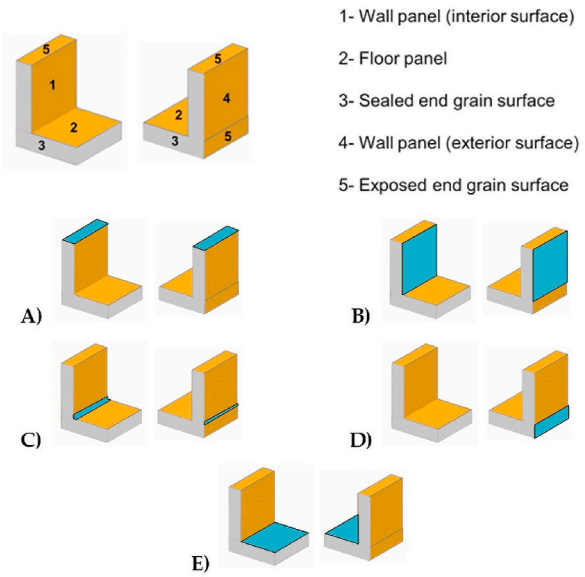

Fig. 1. Wall to floor L-shaped CLT specimens and expected water absorption scenarios. Blue surfaces representing probable absorption surfaces: A) parallel to the grain (end-grain surface) by the wall panel without moisture trapping; B) perpendicular to the grain by the wall panel; C) parallel to the grain (end-grain surface) by the wall panel with moisture trapping; D) parallel to the grain (end-grain surface) by the floor panel; E) perpendicular to the grain by the floor panel. (colour). (For interpretation of the references to colour in this figure legend, the reader is referred to the Web version of this article.)

construction schedule. When possible, it is advisable to make decisions based on meteorological data indicating the probability of events that can lead to the environmental conditions conducive to wood degradation.

One possibility for assessing the risk of biological degradation based on geographical location is the model proposed by Scheffer (1971) [39]. The model defines the relative risk of fungal degradation based on average temperature and the number of rainy days, translated into a number called Scheffer's Climate Index (SCI). The model is based on exposure conditions that lead to favourable conditions for the proliferation and development of decay fungi. MC, relative humidity of the air, and ambient temperature are key factors in degradation by decay fungi. There isn't a threshold that determines if an attack will occur, as it depends on the species of wood and fungus [40]. However, degradation will only begin if the wood reaches a moisture content of approximately 20 %, with optimal values above 50 %, and in ideal temperature conditions between 10 and 30 °C, with development uncommon at temperatures below 0 °C or above 40 °C [6,41].

From the SCI, maps of areas with higher risks of degradation were created for different regions, countries, and even continents around the world, such as Canada [42], Japan [43], Australia [44], Norway [45], North America [46], and Europe [47]. However, it is necessary to emphasize that the model proposed by Scheffer (1971) [39] is used to assess the relative risk of sawn timber exposed to outdoor conditions (Use Class 3 [48]) in a long-term perspective, and most structural EWP are designed to serve in Use Class 2 [48], being exposed to a Use Class 3 only during the construction phase, in other words, in a short-term perspective.

Portugal has shown a growing interest in MTB construction, increasingly opening automated and technological factories for local production of EWPs such as CLT and increasing the number and complexity of wooden constructions in the country. However, most MTBs and EWPs are built and sourced from companies in Central and Northern Europe, without any adaptation to the Portuguese climate. Therefore, it is of paramount importance to analyse the risks associated with the Portuguese climate, as it is a temperate and highly variable climate.

The main objective of this work is to evaluate the risks associated with exposure to rain of CLT structural elements. For this purpose, initial results of environmental exposure tests of CLT Wall-Floor connection specimens are presented and analysed, through the identification of critical zones, the detection of details contributing to moisture absorption and entrapment, and the evaluation of damages caused by four months of exposure. Additionally, the paper will present a degradation risk map for Portugal's mainland using the model proposed by Scheffer (1971) [39] which may be used as a reference in preliminary analysis for decision-making regarding necessary moisture control and protection measures on-site.

2. Materials and methods

2.1. Environmental exposure tests of CLT wall to floor joints

The CLT used to build the specimens was composed of five layered Norway Spruce (*Picea abies* Karst.) panels with 500 × 500 × 126 mm^3. Before the exposure, all specimens were stored in a climatic chamber (temperature of 20 ± 1 °C and relative humidity of 60 ± 5

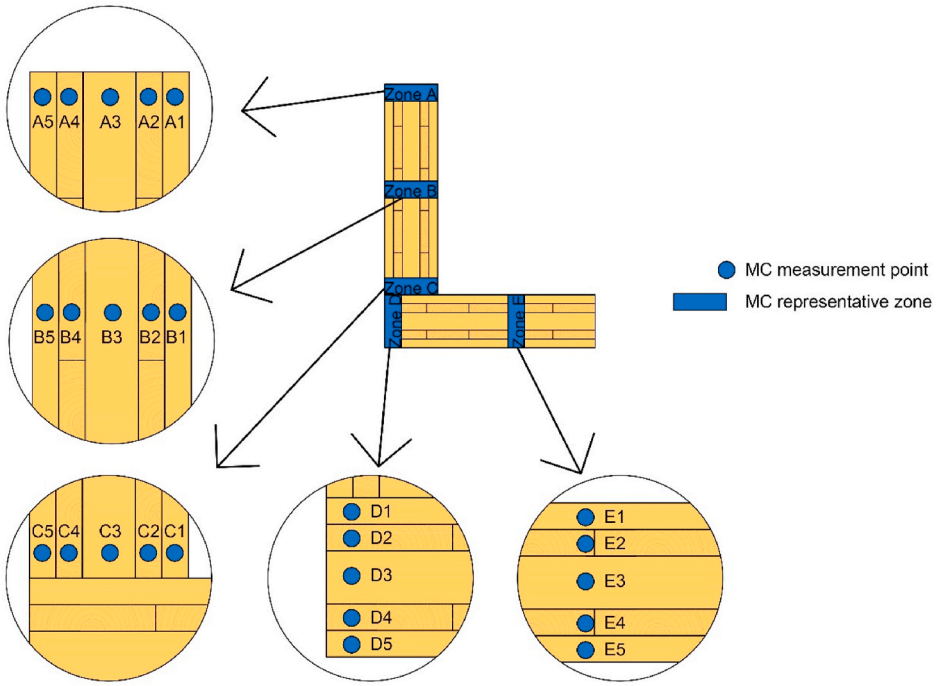

Fig. 2. Moisture content monitorization scheme. (colour). (For interpretation of the references to colour in this figure legend, the reader is referred to the Web version of this article.)

%) until mass stabilization (difference ≤0.1 % between consecutive measurements). According to the equation to calculate the Equilibrium Moisture Content (EMC) provided by Glass et al. (2021) [49], the climatic condition of the climatic chamber corresponds to an EMC between 10.1 % and 12.0 %.

The natural exposure setup consisted of one set of four specimens directly exposed to outdoor weather on the rooftop of a building at the University of Minho, Guimarães, Portugal. The specimens are L-shaped specimens that represent the connection between a facade wall panel and a floor panel. This configuration was adopted because it represents a critical zone of water accumulation [18, 50]. Therefore, the specimen is composed of two CLT panels connected to mimic the exterior wall to the intermediate floor joint. To limit water infiltration to the surfaces that are exposed in real cases, three surfaces of the floor panel and two of the wall panel were sealed with impermeable painting (Fig. 1). The top surface of the wall panel was left unsealed to represent a window opening. This way, the specimen represents five water absorption scenarios – A) parallel to the grain (end-grain surface) by the wall panel without moisture trapping; B) perpendicular to the grain by the wall panel; C) parallel to the grain (end-grain surface) by the wall panel with moisture trapping; D) parallel to the grain (end-grain surface) by the floor panel; E) perpendicular to the grain by the floor panel (Fig. 1).

The environmental conditions (temperature, relative humidity, precipitation, and wind speed) and the wood MC were monitored. The external climatic variables were obtained from a weather station located on a neighbouring building within the University of Minho campus, and the monitorization of the MC was based on the electrical resistance method, which allows obtaining the MC in specific locations inside the panels and verifying areas of moisture accumulation and moisture gradients.

The electrical resistance method only performs measurements representative of that point. Therefore, to obtain representative measurements of the specimen, it was necessary to measure the MC in different layers (to observe the moisture gradient) and zones along the panels. Therefore, electrodes were installed to measure all infiltration scenarios exposed in Fig. 1 for all five layers of the CLT. In total, each specimen had 25 measurement points. Fig. 2 shows the 25 MC monitoring points, where the nomenclature is defined based on an alphanumeric code composed of a letter and a number. The letter refers to the water absorption scenario shown in Fig. 1, and the number refers to the CLT layer where layers 1 and 5 are the outermost layers and layer 3 is the central layer. The measurement frequency varied according to the climatic variation and the observed response in the last MC measurements and was done manually. The exposure began on January 10, 2024, and the data presented in this paper is from a short-term perspective, such as in a normal humidification situation during construction (sixteen weeks of exposure).

2.2. The wood biological degradation risks considering the Portuguese mainland climate

In this study, the SCI [39] will be the index used to quantify the risk of fungal degradation relative to geographical location, calculated from equation (1). Where T represents the monthly average temperature, in °C and D the number of days with rainfall equal to or above 0.25 mm.

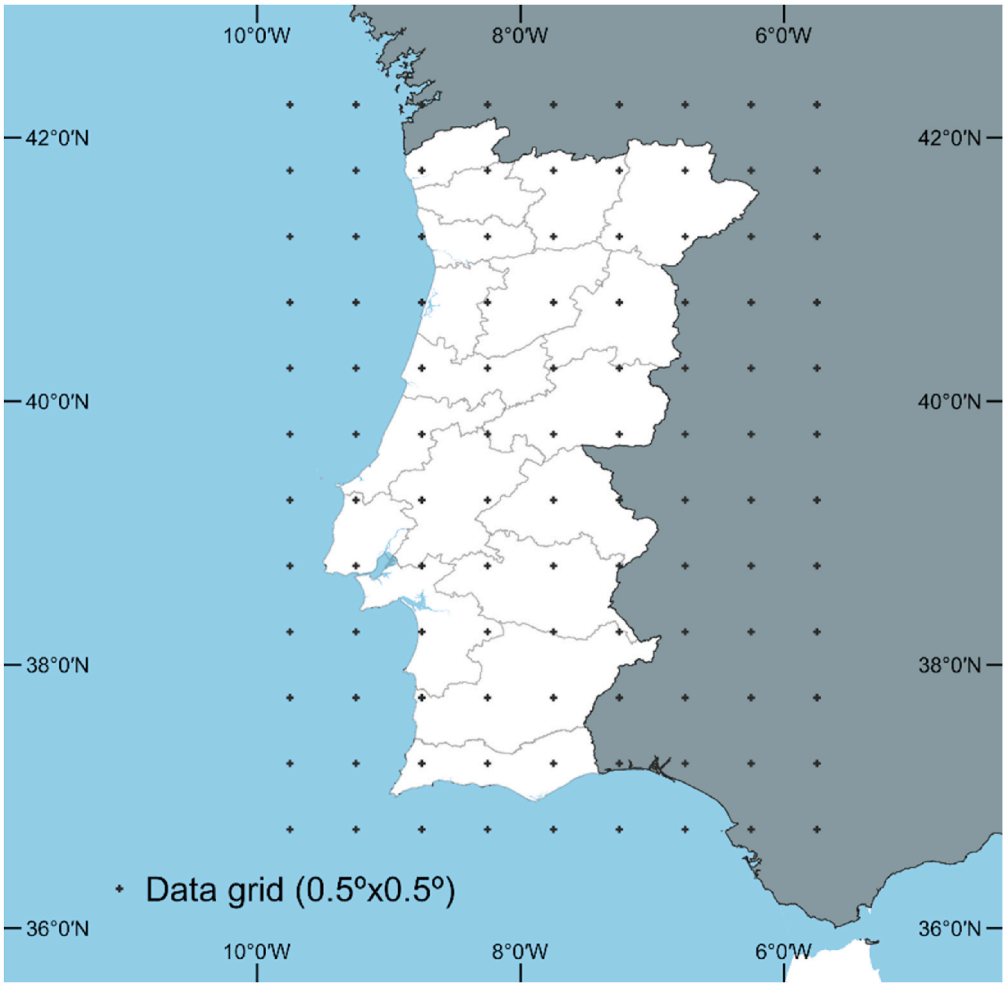

Fig. 3. Monthly average temperature and daily precipitation dataset grid. (colour). (For interpretation of the references to colour in this figure legend, the reader is referred to the Web version of this article.)

$$SCI = \frac{\sum_{Jan.}^{Dec.}[(T-2)(D-3)]}{16.7} \quad (1)$$

The choice of using Scheffer's model in this study was based on the availability of input data, model complexity, its adaptability, and because it presents the outputs more clearly and directly, in addition to being a well-established and widely disseminated model, thereby fulfilling the study's objective of providing a simple decision-making tool for designers and builders in the preliminary phases (Design Phase and Construction Phase) of an MTB. It is worth noting that the model can only be used for comparison between different locations, and it is not possible to determine if degradation will occur or to define any degradation rate from the SCI.

One of the difficulties in mapping the SCI is the need for a long series of accurate meteorological data (monthly temperature and daily precipitation) at various points in the mapped area. In many regions, the available data are of inadequate temporal resolution, low quality, or even non-existent. In this regard, resorting to meteorological data from satellite-based reanalysis has become increasingly common (e.g. Refs. [51–54]).

The input meteorological parameters were obtained from the NASA Prediction of Worldwide Energy Resource (NASA POWER) database. Despite various reanalysis databases' existence, NASA POWER stands out for its user-friendly interface, providing a vast array of data with spatial resolution of 0.5° latitude by 0.5° longitude and temporal resolution of days, months or years. Therefore, the mapping was carried out based on a data grid (monthly average temperature and daily precipitation) with a resolution of 0.5° by 0.5° (Fig. 3) starting on January 1, 1991, and ending on December 31, 2020 (30 years).

After calculating the SCI from equation (1) for each point shown in Fig. 3, the data were interpolated using the Triangulated Irregular Networks (TIN) automated routine in the QGIS georeferencing software.

Despite some studies pointing to the reliability of data provided by the NASA POWER project [51,52], a verification of the data was conducted by comparing it with data from 13 weather stations available at the Portuguese Institute for Sea and Atmosphere (IPMA) website, considered as reference data. Precipitation data is not available at the daily resolution; therefore, monthly data was used to

Table 1
Information about the 13 weather stations used for data verification.

Weather Stations	Latitude	Longitude	Altitude	Temporal range
Beja	38°1′N	7°52′W	246m	Jan/1981–Dec/2018
Bragança	41°48′N	06°44′W	690m	Jan/1981–Dec/2018
Castelo Branco	39°50′N	7°28′W	386m	Jan/1981–Dec/2018
Coimbra	40°12′N	8°25′W	74m	Jan/1981–Dec/1995
Evora	38°34′N	7°54′W	309m	Jan/1981–Sep/2008
Faro	37°1′N	7°58′W	74m	Jan/1981–Dec/2018
Lisboa	38°42′N	9°08′W	77m	Jan/1981–Dec/2018
Montalegre	41°49′N	7°47′W	1005m	Jan/1981–Dec/2018
Penhas Douradas	40°25′N	7°33′W	1380m	Jan/1981–Dec/2018
Portalegre	39°17′N	7°25′W	597m	Jan/1981–Dec/2018
Porto	41°08′N	8°36′W	93m	Jan/1981–Dec/2010
Santarém	39°12′N	8°44′W	73m	Jan/1981–Dec/2018
Setúbal	38°32′N	8°53′W	35m	Jan/1981–Dec/2018

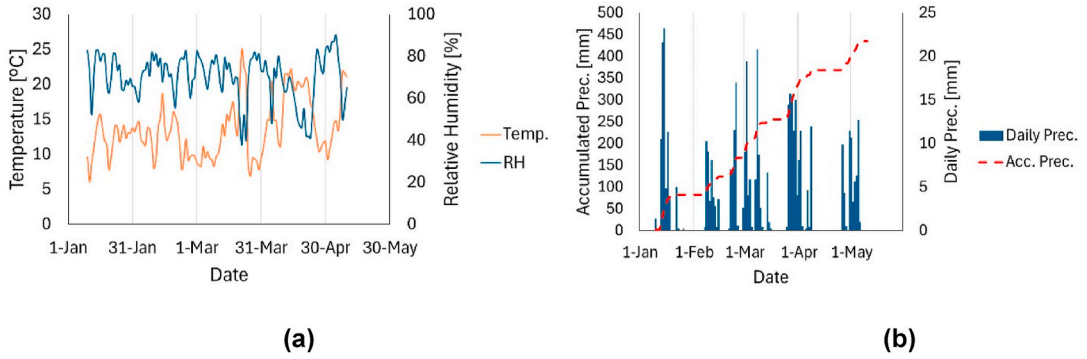

Fig. 4. Environmental exposure conditions recorded by the weather station installed at the University of Minho: (a) Temperature and Relative Humidity; (b) Daily and accumulated precipitation. (colour). (For interpretation of the references to colour in this figure legend, the reader is referred to the Web version of this article.)

verify precipitation. The comparison methodology was based on Rodrigues & Braga (2021) [51] and Tayyeh & Mohammed (2023) [52]. The coefficient of determination (R2), the mean bias error (MBE), and the Nash and Sutcliffe [55] modelling efficiency (EF) were calculated from equations (2)–(4), respectively.

$$R^2 = \left[\frac{\sum_{i=1}^{n} (O_i - O_a)(R_i - R_a)}{\left[\sum_{i=1}^{n} (O_i - O_a)^2\right]^{0.5} \left[\sum_{i=1}^{n} (R_i - R_a)^2\right]^{0.5}} \right]^2 \tag{2}$$

$$MBE = \frac{\sum_{i=1}^{n} R_i - O_i}{n} \tag{3}$$

$$EF = 1 - \frac{\sum_{i=1}^{n} (O_i - R_i)^2}{\sum_{i=1}^{n} (O_i - O_a)^2} \tag{4}$$

Where O_i is the data observed by the IPMA station, O_a is the average of the observed data for a given station, R_i is the data obtained from the NASA POWER reanalysis for the location of the meteorological station, R_a is the average of the reanalysis data for a given point, and n is the number of samples.

The R^2 is a numerical measure ranging from 0 to 1, where the closer to 1, the better the data fits a linear regression. Evaluating the R^2 is often complex and varies depending on the measure analysed. In this study, a R^2 value above 0.75 was considered a strong fit to the linear model [51]. Regarding MBE, it indicates whether the model overestimates (positive MBE values) or underestimates (negative MBE values) the parameter, with the ideal MBE being zero [56]. Finally, EF is a value that can range from -∞ to 1, with EF = 1 indicating that the observed values (O_i) and the reanalysis values (R_i) are equal [57].

Table 1 presents the weather stations used in data verification, indicating their name, latitude, longitude, altitude, and temporal range.

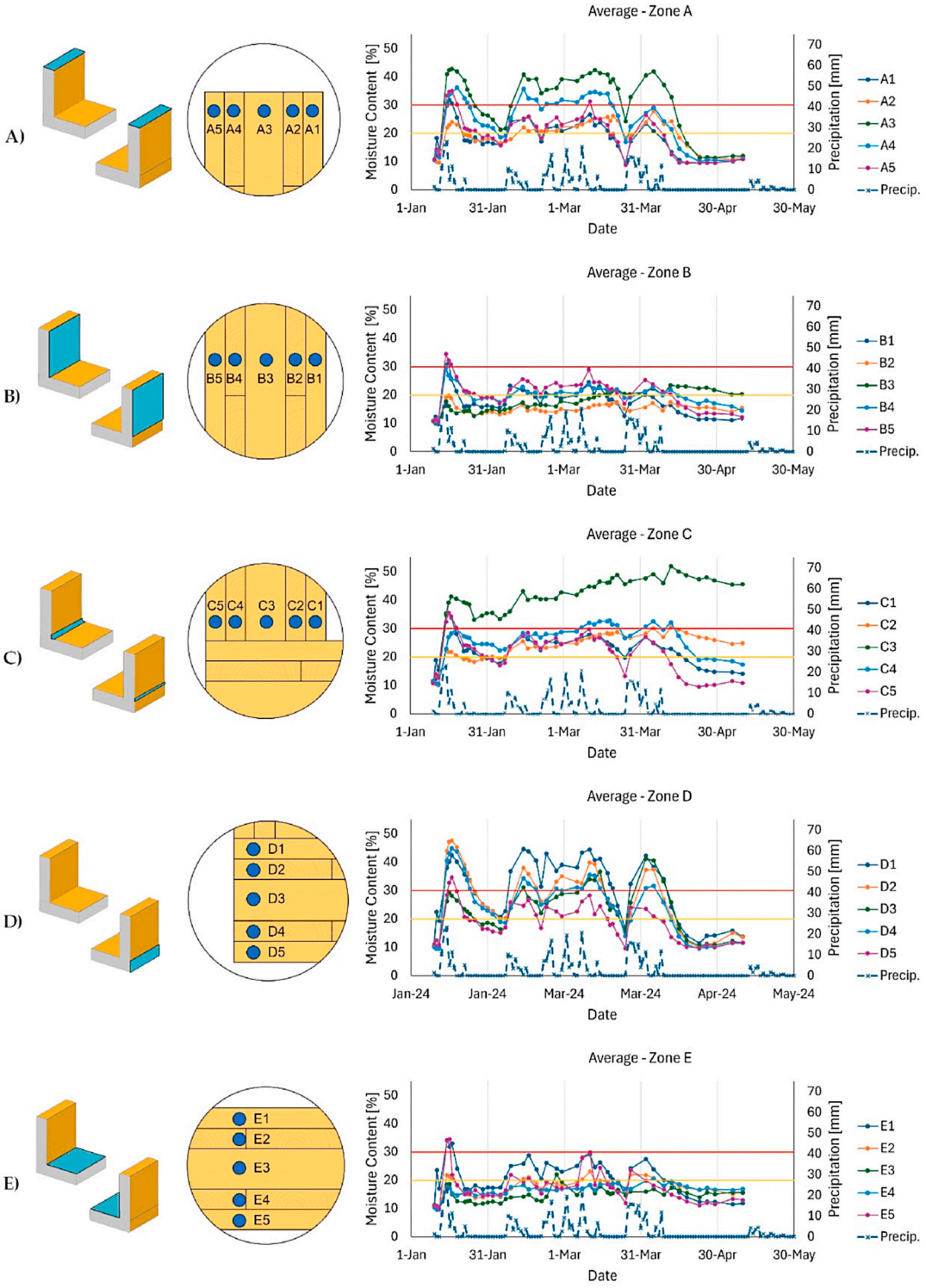

Fig. 5. Average moisture content of the 5 layers of CLT in each of the 5 monitored zones and daily precipitation. (colour). (For interpretation of the references to colour in this figure legend, the reader is referred to the Web version of this article.)

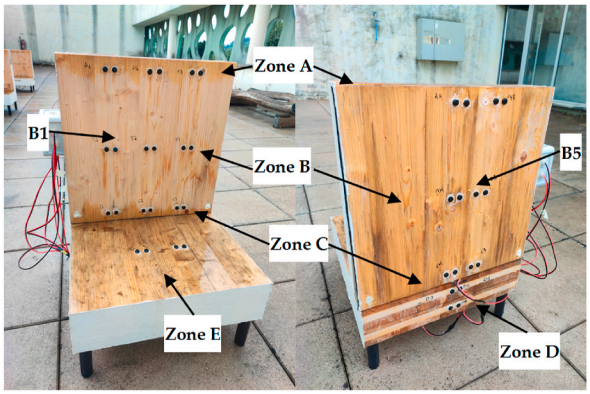

Fig. 6. Wall-floor joint Specimen after rainy period. (colour). (For interpretation of the references to colour in this figure legend, the reader is referred to the Web version of this article.)

3. Results

3.1. Natural exposure tests of CLT wall to floor joints

3.1.1. Exposure climatic conditions

Fig. 4 presents the results of the climatic conditions at the exposure site during the test period. During this period, there was an accumulated precipitation of approximately 435 mm over 63 rainy days, representing 52 % of the exposure period. The recorded average temperature was 13.6 °C, with a daily maximum of 25.1 °C and a minimum of 6.1 °C. The daily relative humidity ranged from 37.6 % to 90.0 %, with an average of 70.0 %.

3.1.2. Moisture content monitorization

Fig. 5 presents the results divided by zones of the average MC for each monitored point, as well as daily precipitation. It highlighted the thresholds of 20.0 % and 30.0 % MC, where 20.0 % represents the average value considered in the literature to initiate the biological degradation process, and 30.0 % represents approximately the fibre saturation point (FSP). Beyond this point, the change in MC does not cause volumetric changes in the wood, and the risk of degradation increases due to the higher presence of free water in the material. Additionally, it represents the point at which the electrical resistance method decreases its measurement accuracy [6,58,59].

Despite the results presented in section 3.1.1 indicating precipitation between April 26 and May 6, the data shown in Fig. 5 considered zero precipitation because the specimens were moved to a covered area for maintenance of the waterproof paint and the monitoring system.

From the analysis of Fig. 5, it can be inferred that the zones with exposed end grain (zones A, C, and D) exhibit a rapid and excessive increase in MC in all five layers, surpassing the 20.0 % threshold in the first days of rain and maintaining it throughout almost the entire rainy periods. In contrast, the zones that allow infiltration only through the outer lamellae (zones B and E) showed rapid absorption in and the surfaces directly exposed to weather (layers 1 and 5), frequently surpassing the 20.0 % threshold during rainy periods, while the other layers exhibited much slower and reduced absorption. Fig. 6 shows a specimen a few hours after the end of a rain event, and it can be inferred from Figs. 5 and 6 that the direction of the rain affects only zone B, with a higher MC in layer B5 when compared to layer B1.

Regarding the drying behaviour, Fig. 7 presents the MC over time, starting on March 31 and ending on May 10, which marks the last drying cycle observed in this first exposure phase. Additionally, the Equilibrium Moisture Content (EMC) was calculated based on the daily values of temperature and relative humidity using the equation presented by Glass et al. (2021) [49]. It can be seen in Fig. 7 that, despite zones A and D exhibiting rapid and excessive humidification due to exposed end grain, their drying out is also faster. All layers in zones A and D show an average MC below 20.0 % after approximately 16 and 13 days, respectively. Zone E, when disregarding potential infiltrations through panel failures, presented drying of all lamellas to safe MC levels after approximately 10 days. Despite having lower MC than zones A and D, Zone B showed resistance to drying in the central lamella (B3), which maintained an average MC of 20.3 % even after 39 days of drying. Finally, zone C was the most critical, as the end grain is sufficiently exposed to allow direct contact with water, and the interface between the wall and floor panel prevents adequate ventilation for drying, resulting in entrapped water, especially in point C3. In zone C, after 39 days of drying, layers C2 and C3 still had average MCs of 24.9 % and 45.6 %, respectively.

Additionally, Figs. 6 and 7 highlight how different parts of the connection impact moisture absorption and drying. The vertical wall panel channels rainwater toward the most absorbent surfaces (end-grain surfaces), while the horizontal floor panel favours the water pooling and hinders the ventilation of the lower part of the wall panel, slowing the drying process.

Despite being beneficial for durability against biological agents, the rapid drying observed in Zones A and D results in moisture gradients and internal stresses in CLT. These, in turn, lead to excessive deformations, drying cracks, and delamination (Fig. 8). These physical damages create pathways for water infiltration into deeper regions, potentially trapping water within the elements and favour

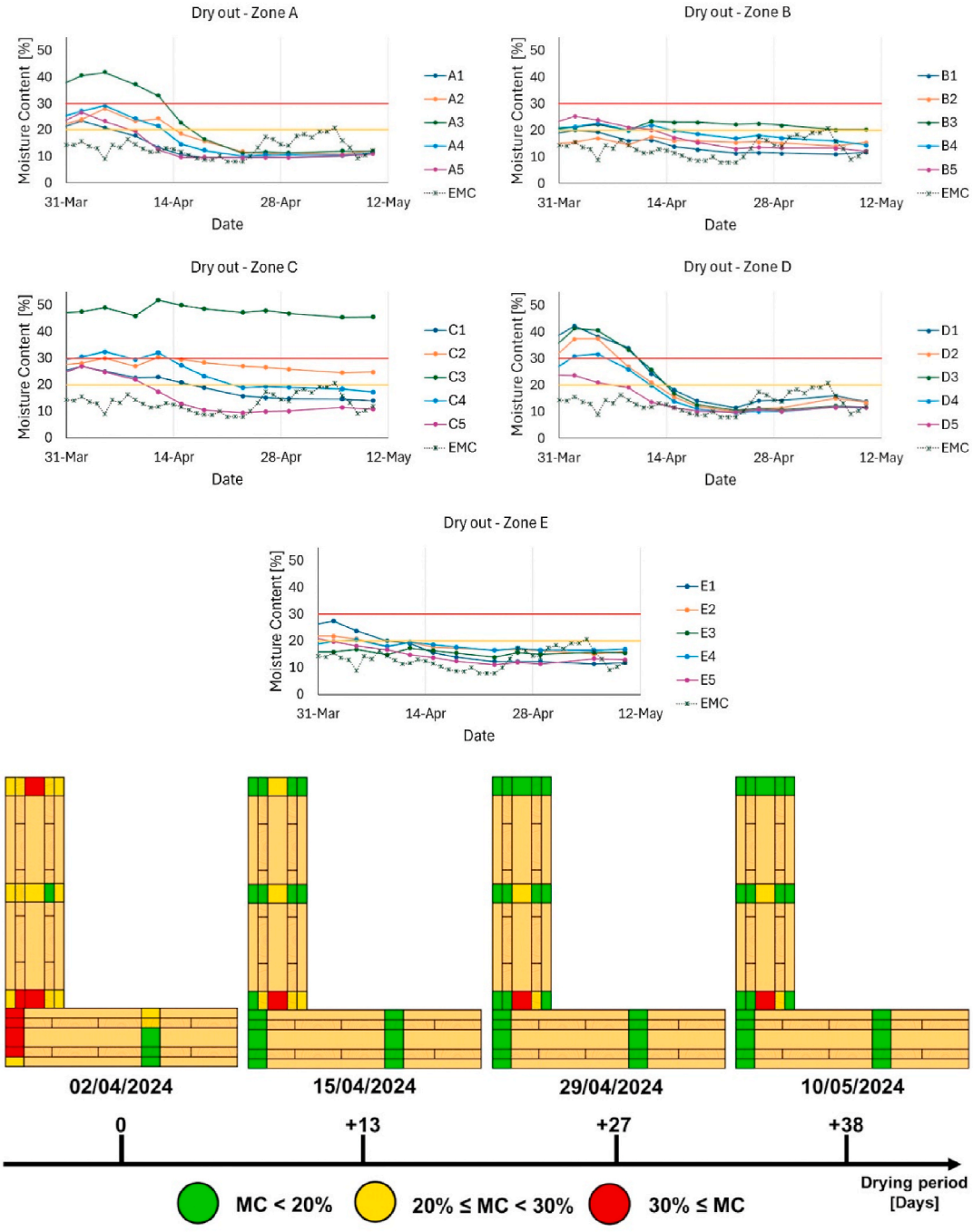

Fig. 7. Wall-floor joint drying behaviour. (colour). (For interpretation of the references to colour in this figure legend, the reader is referred to the Web version of this article.)

the entry and installation of biological degradation agents. This same phenomenon was observed by Kalbe et al. (2022) [18] in areas around window openings (walls) and skylights (roofs) in panels from various suppliers. Therefore, it was attributed to repeated wetting cycles rather than a manufacturing defect.

3.2. The wood biological degradation risks considering the Portuguese mainland climate

3.2.1. NASA POWER data validation

Fig. 9 presents the coefficients of determination (R^2), Mean Bias Error (MBE), and Modelling Efficiency (EF) for the 13 weather

Fig. 8. Delamination, drying cracks, and deformations caused by repeated wetting and drying of the end-grain face: (a) Zone A; (b) Zone B. (colour). (For interpretation of the references to colour in this figure legend, the reader is referred to the Web version of this article.)

stations considered in this study, both for temperature and precipitation data. The R^2 values ranged from 0.94 to 0.99 with an average of 0.98 for temperature data and from 0.81 to 0.93 with an average of 0.87 for precipitation data. Regarding the MBE, for temperature data, the values ranged from −1.98 °C to 2.92 °C with an average of −0.25 °C, while precipitation data showed an average of −14.83 mm, with a maximum of 5.24 mm and a minimum of −46.49 mm. Finally, the EF averaged 0.90 with a maximum of 0.98 and a minimum of 0.68 for temperature and averaged 0.80 with a maximum of 0.89 and a minimum of 0.56 for precipitation.

It can be inferred from the analysis of Fig. 9 that both the temperature and precipitation data provided by the NASA POWER platform have a good correlation with the data recorded at the IPMA climatological stations, as indicated by the high R2 values obtained for all 13 stations. Regarding the MBE, the data show a slight tendency to underestimate the temperature (average MBE of −0.25 °C). It is important to note that stations located in high-altitude regions (Montalegre and Penhas Douradas) exhibit the opposite behaviour, overestimating the average monthly temperature. Conversely, Fig. 9(d) indicates that precipitation tends to be underestimated in higher-altitude regions. Finally, analysing the overall efficiency of the model, the EF values indicate good performance of the NASA POWER data, with some caveats for higher altitude regions, as these areas have a unique microclimate highly influenced by their surroundings.

However, studies indicate that the SCI should be used cautiously in regions with very specific microclimates, such as mountainous areas, where sudden climate variations can occur even over small distances. The Montalegre and Penhas Douradas stations, located in the Serra do Gerês and Serra da Estrela, respectively, fall within regions where the application of the SCI requires special attention [39, 60].

The results obtained align with similar studies, such as Bai et al. (2010) in China [61], Monteiro et al. (2017) in Brazil [62], Al-Kilani et al. (2021) in Jordan [63], Rodrigues & Braga (2021) for the Alentejo region in Portugal [51], Kheyruri & Sharafati (2022) in Iran [64], and Tayyeh & Mohammed (2023) in Iraq [52], indicating its reliability for obtaining temperature and precipitation data for mapping the degradation risk according to Scheffer's model (1971) [39].

3.2.2. Portugal mainland SCI map

Fig. 10a,b,c presents the annual and monthly SCI map for mainland Portugal. The highest degradation risk is found in the central and northern coastal regions, with indices above 80. The risk of degradation gradually decreases as one moves inland, with indices below 55 in almost the entire eastern border with Spain. The SCI map in Fig. 10 may be used as a guide for design precautions or preservative treatments needed for timber construction and can be extended to other locations using equation (1) and data provided by the NASA POWER dataset.

Scheffer (1971) [39] further defines three levels of the index: an SCI below 35 represents the least favourable conditions for degradation (Low risk), an SCI between 35 and 65 represents intermediate conditions for degradation (Medium risk), and an SCI between 65 and 100 represents the favourable conditions for degradation (High risk). Values above 100 are considered Very high-risk areas. It is important to note that in regions with significant elevation changes, such as mountainous areas where temperature and rainfall can vary abruptly, the accuracy of the map is reduced.

The annual risk map reflect the long-term degradation risk, which does not represent the construction period of an MTB. Therefore, the map was divided into 12 separate maps, one for each month of the year, to serve as a reference of climate exposure severity during the construction months to be used by builders and designers.

4. Discussion

Table 2 presents a summary of 6 papers about MC monitorization in EWP directly exposed to rainwater, either through

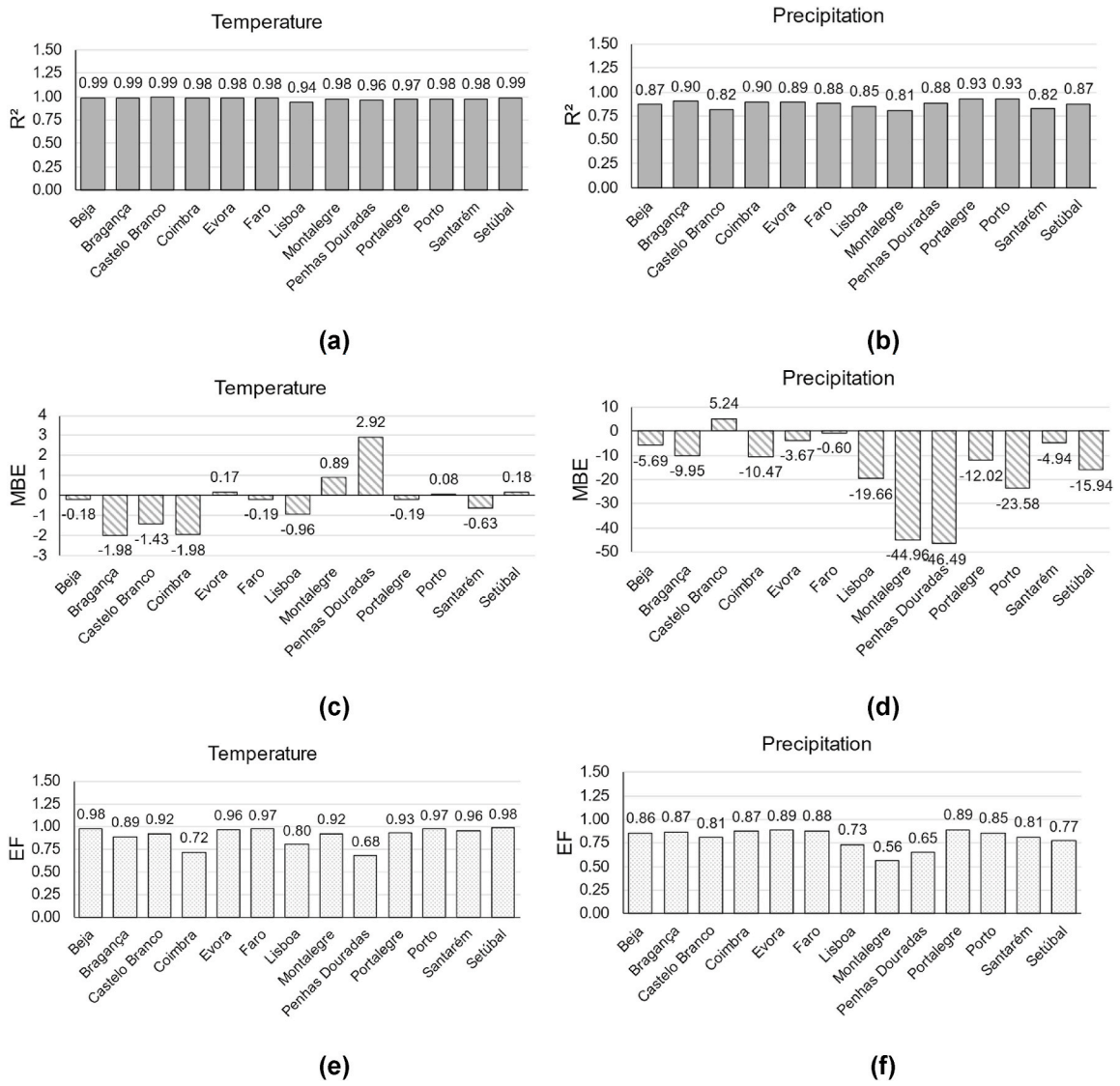

Fig. 9. Results of the NASA POWER data validation: (a) Average monthly temperature coefficient of determination (R^2); (b) Accumulated monthly precipitation coefficient of determination (R^2); (c) Average monthly temperature Mean Bias Error (MBE); (d) Accumulated monthly precipitation Mean Bias Error (MBE); (e) Average monthly temperature Modelling Efficiency (EF); (f) Accumulated monthly precipitation Modelling Efficiency (EF). (colour).

experimental campaigns or case studies. The “EWP Zone” column refers to the water infiltration scenarios shown in Fig. 1, where Zone A represents infiltration through the end-grain face in vertical elements without moisture entrapment, Zone B represents infiltration in vertical elements without exposed end-grain, Zone C represents infiltration through the end-grain face in vertical elements with moisture entrapment, Zone D represents infiltration through the end-grain face in horizontal elements without moisture entrapment, and Zone E represents infiltration in horizontal elements without exposed end-grain. The "Time to reach safe MC" column refers to the MC established by the respective study as safe, ranging from 18 % to 20 %, with some studies not specifying the exact value considered.

A comparative analysis of results obtained from outdoor exposure of specimens is often complex, as the outcomes are directly dependent on the local microclimate, exposure time, and the analysed parameters in each study. Additionally, the lack of standardization between methods complicates this comparative analysis.

However, the results presented in Table 2 are consistent with the findings exposed in Section 3 and show that exposed end-grain faces are indeed the main zones of water infiltration (Zones A, C, and D), quickly reaching MC values above the FSP (around 25.0%–30.0 % [7]) in nearly all the studies presented. Conversely, faces with exposed end-grain but without moisture entrapment (Zones A and D) showed rapid drying within a few days, except for the study published by Liisma et al. [20], where cold and humid climate delayed the dry-out of the panels. Faces with exposed end-grain and moisture entrapment (Zone C) represent the most critical scenario, with excessive humidification and extended time to reach safe MC levels. The results for Zone C also highlight the need for adequate

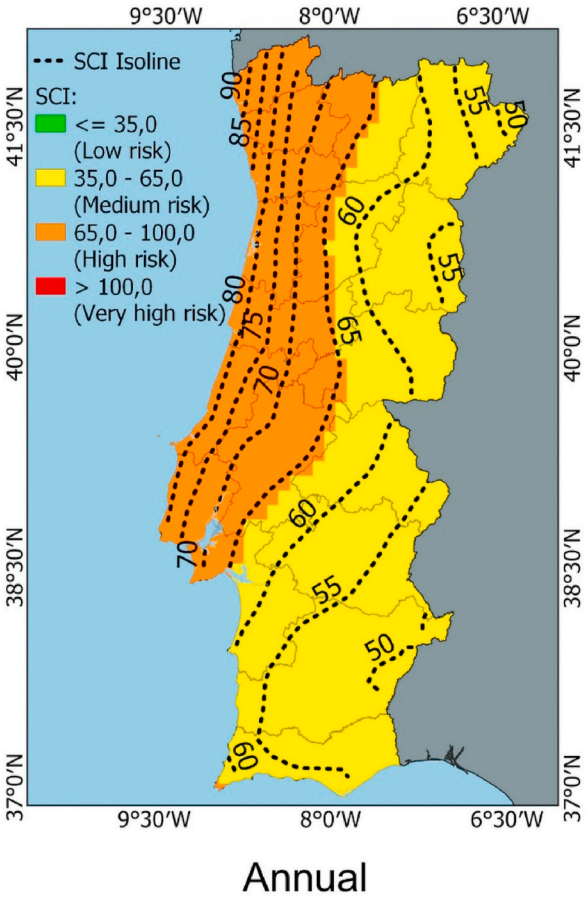

Fig. 10. aPortugal mainland Scheffer's climate index (1991–2020). (Part I). (Colour). (For interpretation of the references to colour in this figure legend, the reader is referred to the Web version of this article.)

drying of the elements before proceeding with the application of subsequent layers, as materials from Zone A or D can turn into Zone C, drastically reducing their drying capacity.

Regarding the drying of panels, Kalbe et al. (2022) [18] observed that in one case study, panel drying was only achievable through intensive mechanical drying. However, such methods resulted in the formation of large and visible drying cracks on the panel surfaces. Shirmohammadi & Faircloth (2023) [65] analysed the drying of CLT panels using fans and concluded that the face exposed to the drying equipment dried quickly, but the internal layers of the panel remained wet. Therefore, the best approach is to protect the panels from rain during construction, and in case of protection system failure, mechanical drying can serve as a mitigation measure.

Although using full temporary shelter throughout the construction phase is ideal for keeping EWP dry, it can often be costly and overly protective. In this context, Alsmarker (2022) [22] provides a practical guide on how to protect critical details of CLT panels during construction when using full-time shelter is neither possible nor necessary. In his book, Alsmarker (2022) [22] specifies how to protect element joints, wall-to-floor and wall-to-foundation connections, balconies and balcony access points, door and window openings, stairwells, shafts, and cut-offs. In cases where full temporary shelter is not feasible, the following recommendations should be considered [22,66].

- Store EWP protected from rain, sun, and dirt, ensuring adequate ventilation.
- Protect end-grain surfaces, element joints, and connections with breathable damp-proof membranes or tapes.
- Remove standing free water or snow from horizontal surfaces as quickly as possible.
- Allow adequate drying in case of humidification and ensure that infiltrated water can drain.
- Perform encapsulation only after the proper drying (MC $\leq$ 18 %).
- Continuously monitor the MC throughout the construction process.

However, the decision to invest in a permanent shelter for the construction phase should be based on the severity of exposure during the construction period. For example, in the case of construction expected to last six months (the period between the start of assembly and the end of permanent protection of the EWPs) scheduled to begin in June in the southern region of mainland Portugal,

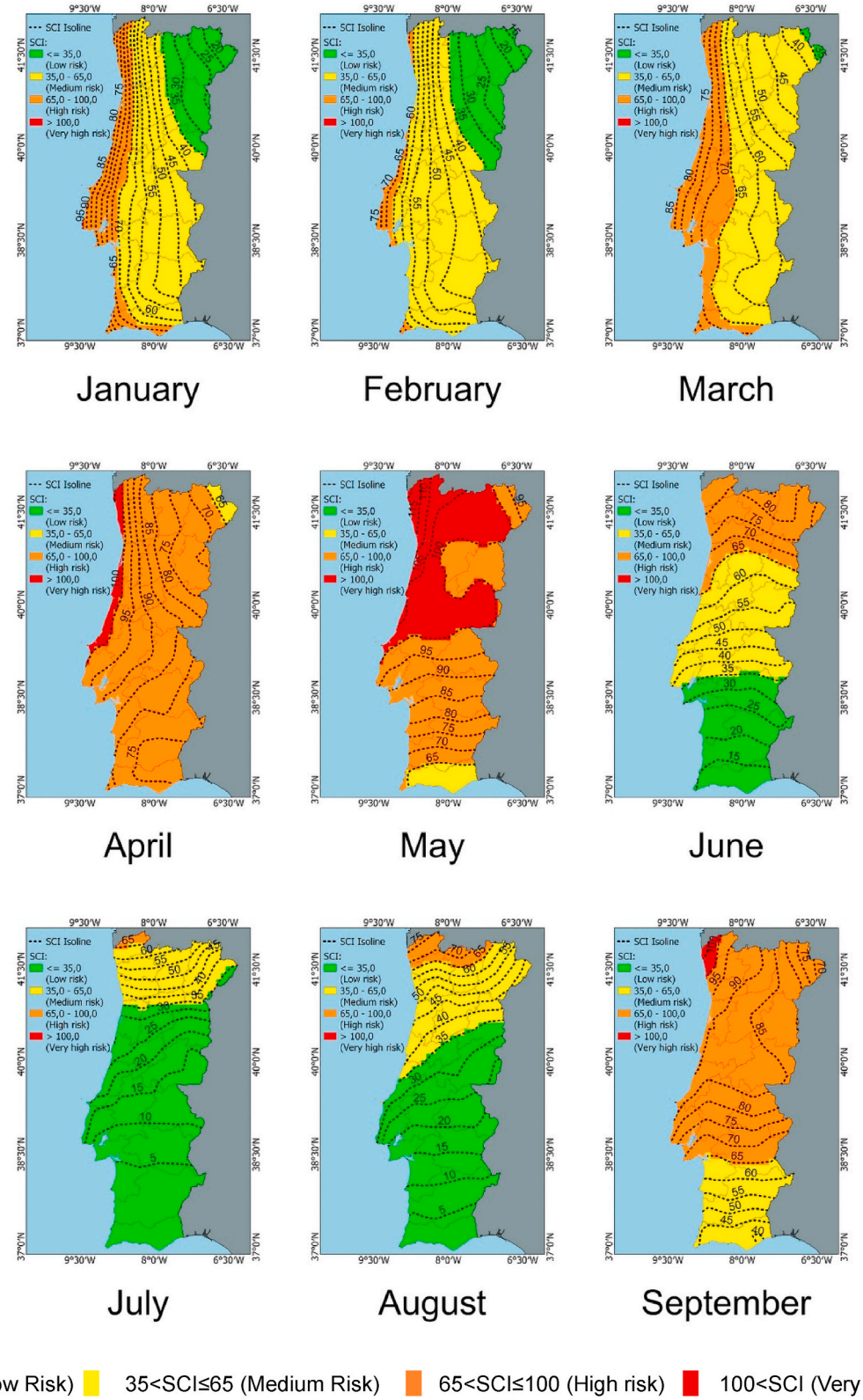

Fig. 10. bPortugal mainland Scheffer's climate index (1991–2020. (Part II). (Colour). (For interpretation of the references to colour in this figure legend, the reader is referred to the Web version of this article.)

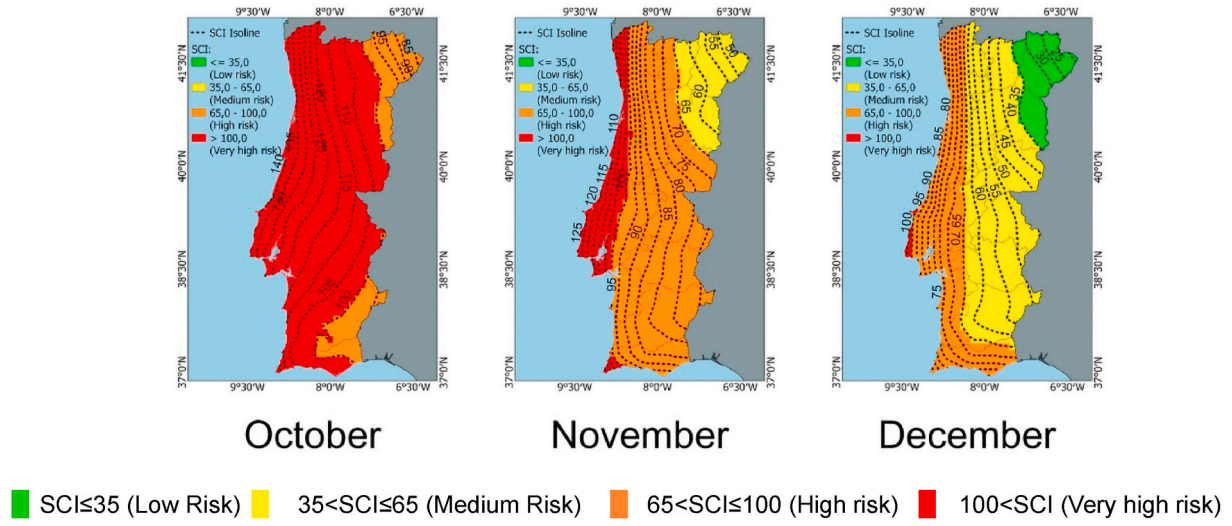

Fig. 10. cPortugal mainland Scheffer's climate index (1991–2020. (Part III). (Colour). (For interpretation of the references to colour in this figure legend, the reader is referred to the Web version of this article.)

Table 2
Summary of results obtained in studies about MC monitorization of EWPs exposed to rainwater.

Reference	Type of data	Exposure time	Precipitation	EWP Zone	Max MC	Time to reach safe MC
Schmidt et al. (2019) [31]	Case study	–	179 mm	A	45.0 %	–
				C	24.0 %	4 months
Liisma et al. (2019) [20]	Experimental	8 weeks	90 mm	C	Above 25.0 %	Still wet at the end of the experiment
				D	Above 25.0 %	1 month
Austigard & Mattson (2020) [32]	12 Case Studies	–	–	–	Above FSP	Still wet after 5 months
Kalbe et al. (2021) [17]	Experimental	1 week	–	C	Above 30.0 %	Still wet after 15 days
Kalbe et al. (2022) [18]	6 Case studies	1–21 weeks	14–335 mm	C	Above 40.0 %	2.5–6 months
				D	Above 40.0 %	Rapid dry out
				A	Above 40.0 %	–
Li et al. (2023) [16]	Experimental	–	–	A	30.0–35.0 %	2 days
				B	20.0–25.0 %	2 days
Lima et al. (2024) Present Study	Experimental	16 weeks	435 mm	A	42.8 %	13–16 days
				B	34.4 %	Still wet after 39 days
				C	51.9 %	Still wet after 39 days
				D	47.6 %	10–13 days
				E	34.5 %	7–10 days

Fig. 10 indicates that during the first four months, the use of full temporary shelter may be excessive, and its placement can be postponed until the last two months of construction. Conversely, for the same construction taking place on the northwest coast of mainland Portugal, Fig. 10 suggests that it may be advisable to use full temporary shelter throughout the entire construction period.

5. Conclusions

The primary objective of this paper was to discuss the risks associated with rain exposure of CLT elements during the construction phase based on the results of 16 weeks exposure of CLT specimens. Key findings include.

- Exposed end-grain faces are the primary zones of water absorption, quickly reaching MC levels above the FSP.
- End-grain faces without moisture entrapment (Zones A and D) exhibited rapid drying but presented severe physical damages such as delamination, cracks, and warping.
- End-grain faces with moisture entrapment (Zone C) showed almost no drying capacity.
- Zones B and E exhibited slower absorption but were prone to moisture entrapment in the inner layers.

Protective measures against weather exposure should be defined according to the project's budget and the severity of the exposure climate during construction. Therefore, this study also developed two biological degradation risk maps using data provided by the NASA POWER project, one for long-term exposure (annual map) and one for short-term construction-phase exposure (monthly map).

It is worth mentioning the importance of the acquisition of hygrothermal data (MC, temperature, and relative humidity of the air)

from various exposure conditions (use classes-EN 335 [48]) in Portugal, to build a solid database for the development of predictive models and tools, or the improvement of existing ones (e.g. Ref. [67]), that can quantify the long-term deterioration in the Portuguese context.

In conclusion, moisture control during the construction phase of MTB is critical for maximizing long-term performance. To achieve this, it is necessary to raise awareness among key decision-makers (owners, builders, and designers) about the risks and consequences of prolonged exterior exposure of EWP.

CRediT authorship contribution statement

Daniel F. Lima: Writing – review & editing, Writing – original draft, Visualization, Methodology, Investigation, Formal analysis, Data curation, Conceptualization. **Sónia Duarte:** Writing – review & editing, Methodology, Investigation, Formal analysis. **Jorge M. Branco:** Writing – review & editing, Supervision, Resources, Investigation, Funding acquisition, Formal analysis, Conceptualization. **Lina Nunes:** Methodology, Conceptualization, Supervision.

Funding

This research was supported by the doctoral grant PRT/BD/152833/2021, attributed to the 1st author (D.F.L.), financed by the Portuguese Foundation for Science and Technology (FCT), with funds from the State Budget and the community budget through the European Social Fund (ESF), under MIT Portugal Program.

Declaration of competing interest

The authors declare that they have no known competing financial interests or personal relationships that could have appeared to influence the work reported in this paper.

Acknowledgments

This work was partly financed by FCT/MCTES through national funds (PIDDAC) under the R&D Unit Institute for Sustainability and Innovation in Structural Engineering (ISISE), under reference UIDB/04029/2020 (doi.org/10.54499/UIDB/04029/2020), and under the Associate Laboratory Advanced Production and Intelligent Systems ARISE under reference LA/P/0112/2020. The authors would like to thank the company Arolla for donating the specimens used in the experimental campaign and to acknowledge the technical support and knowledge shared by Richard Santner from Arolla in the analysis of the results.

Data availability

Data will be made available on request.

References

[1] P. Hamburg, K. in Lellep, M. Kiisa, International Study on Best Practices and Knowledge Gaps for Construction of High-Rise Timber Buildings, TTK University of Applied Sciences, Tallin, 2018, https://doi.org/10.13140/RG.2.2.14994.79049.
[2] D.F. Lima, J.M. Branco, L. Nunes, O desafio da durabilidade na construção em altura com madeira, in: J. Aguiar, A. Camões, R. Eires, S. Cunha, R. Malheiro (Eds.), Congresso Construção 2022, Guimarães, 2022, pp. 131–138.
[3] R. Brandner, G. Flatscher, A. Ringhofer, G. Schickhofer, A. Thiel, Cross laminated timber (CLT): overview and development, European Journal of Wood and Wood Products 74 (2016) 331–351, https://doi.org/10.1007/s00107-015-0999-5.
[4] A.C. Woodard, H.R. Milner, Sustainability of timber and wood in construction, in: Sustainability of Construction Materials, Elsevier, 2016, pp. 129–157, https://doi.org/10.1016/B978-0-08-100370-1.00007-X.
[5] A. Stocchero, J.K. Seadon, R. Falshaw, M. Edwards, Urban Equilibrium for sustainable cities and the contribution of timber buildings to balance urban carbon emissions: a New Zealand case study, J. Clean. Prod. 143 (2017) 1001–1010, https://doi.org/10.1016/j.jclepro.2016.12.020.
[6] H. Cruz, D. Jones, L. Nunes, Wood, in: Materials for Construction and Civil Engineering, Springer International Publishing, Cham, 2015, pp. 557–583, https://doi.org/10.1007/978-3-319-08236-3_12.
[7] D.F. Lima, M. Tenório, J.M. Branco, L. Nunes, The wood moisture factor on the biological deterioration of wooden structures, in: Rehabend - Construction Pathology, Rehabilitation Technology and Heritage Management, Granada, 2022, pp. 690–697.
[8] J. Cappellazzi, M.J. Konkler, A. Sinha, J.J. Morrell, Potential for decay in mass timber elements: a review of the risks and identifying possible solutions, Wood Mater. Sci. Eng. 15 (2020) 351–360, https://doi.org/10.1080/17480272.2020.1720804.
[9] M.H. Ramage, H. Burridge, M. Busse-Wicher, G. Fereday, T. Reynolds, D.U. Shah, G. Wu, L. Yu, P. Fleming, D. Densley-Tingley, J. Allwood, P. Dupree, P. F. Linden, O. Scherman, The wood from the trees: the use of timber in construction, Renew. Sustain. Energy Rev. 68 (2017) 333–359, https://doi.org/10.1016/j.rser.2016.09.107.
[10] C. Silva, J.M. Branco, Z. Mehdipour, J. Xavier, P.B. Lourenço, Experimental stress analysis of cross-laminated timber elements under cyclic moisture, J. Mater. Civ. Eng. 34 (2022), https://doi.org/10.1061/(ASCE)MT.1943-5533.0004336.
[11] M. Riggio, N. Alhariri, E. Hansen, Paths of innovation and knowledge management in timber construction in North America: a focus on water control design strategies in CLT building enclosures, Architect. Eng. Des. Manag. 16 (2020) 58–83, https://doi.org/10.1080/17452007.2019.1617672.
[12] M. Riggio, M. Mrissa, M. Krész, J. Včelák, J. Sandak, A. Sandak, Leveraging structural health monitoring data through avatars to extend the service life of mass timber buildings, Front Built Environ 8 (2022), https://doi.org/10.3389/fbuil.2022.887593.
[13] K.E. Udele, A. Sinha, J.J. Morrell, Effects of Re-drying on properties of cross laminated timber (CLT) connections, J. Build. Eng. 76 (2023), https://doi.org/10.1016/j.jobe.2023.107298.

[14] S. Bora, A. Sinha, A.R. Barbosa, Effect of short-term simulated rain exposure on the performance of cross-laminated timber angle bracket connections, J. Architect. Eng. 28 (2022), https://doi.org/10.1061/(asce)ae.1943-5568.0000560.
[15] C. Brischke, G. Alfredsen, Wood-water relationships and their role for wood susceptibility to fungal decay, Appl. Microbiol. Biotechnol. 104 (2020) 3781–3795, https://doi.org/10.1007/s00253-020-10479-1/Published.
[16] K.F. Li, D.P. Fang, K. Habtie, B. Vanderschelden, X. Jiang, L. De Ligne, J. Van Den Bulcke, J. Van Acker, N. Van Den Bossche, Hygrothermal performance of CLT subjected to rain loads during construction in Belgium, in: XVI International Conference on Durability of Building Materials and Components, 2023.
[17] K. Kalbe, A. Annuk, A. Ruus, T. Kalamees, Experimental analysis of moisture uptake and dry-out in CLT end-grain exposed to free water, in: J Phys Conf Ser, IOP Publishing Ltd, 2021, https://doi.org/10.1088/1742-6596/2069/1/012050.
[18] K. Kalbe, T. Kalamees, V. Kukk, A. Ruus, A. Annuk, Wetting circumstances, expected moisture content, and drying performance of CLT end-grain edges based on field measurements and laboratory analysis, Build. Environ. 221 (2022), https://doi.org/10.1016/j.buildenv.2022.109245.
[19] F. Brandstätter, K. Kalbe, M. Autengruber, M. Lukacevic, T. Kalamees, A. Ruus, A. Annuk, J. Füssl, Numerical simulation of CLT moisture uptake and dry-out following water infiltration through end-grain surfaces, J. Build. Eng. 80 (2023) 108097, https://doi.org/10.1016/j.jobe.2023.108097.
[20] E. Liisma, B.L. Kuus, V. Kukk, T. Kalamees, A case study on the construction of a clt building without a preliminary roof, J. Sustain. Architect. Civ. Eng. 25 (2019) 53–62, https://doi.org/10.5755/j01.sace.25.2.22263.
[21] A.J. Prieto, A. Silva, Service life prediction and environmental exposure conditions of timber claddings in South Chile, Build. Res. Inf. 48 (2020) 191–206, https://doi.org/10.1080/09613218.2019.1631143.
[22] T. Alsmarker, Moisture-proof CLT Construction without a Full Temporary Shelter, first ed., Swedish Forest Industries Federation, Stockholm, 2022.
[23] E.L. Schmidt, M. Riggio, A.R. Barbosa, I. Mugabo, Environmental response of a CLT floor panel: lessons for moisture management and monitoring of mass timber buildings, Build. Environ. 148 (2019) 609–622, https://doi.org/10.1016/j.buildenv.2018.11.038.
[24] EN 1995-1-1, Eurocode 5 – Design of Timber Structures – Part 1.1: General – Common Rules and Rules for Buildings, European Committee for Standardization, Brussels, 2004.
[25] EN 16351, Timber Structures - Cross Laminated Timber – Requirements, European Committee for Standardization, Brussels, 2015.
[26] M. Kymäläinen, T. Belt, H. Seppäläinen, L. Rautkari, Decay resistance of surface carbonized wood, Materials 15 (2022) 8410, https://doi.org/10.3390/ma15238410.
[27] Y.-Q. Wu, W.-X. Peng, Y. Qing, Z.-Y. Qin, C.-H. Yao, Y.-L. Feng, Study on energy saving of Chinese-fir wood carbonization process based on moisture absorption characteristics, in: 2009 Asia-Pacific Power and Energy Engineering Conference, IEEE, 2009, pp. 1–4, https://doi.org/10.1109/APPEEC.2009.4918813.
[28] Y. Zhao, Z. Lou, Q. Wang, T. Yuan, M. Chen, H. Han, X. Wu, L. Xu, Y. Li, Fabrication of a bamboo-based glulam based on reconstitution unit innovation: mechanical property investigation and carbon footprint evaluation, Ind. Crops Prod. 202 (2023) 117046, https://doi.org/10.1016/j.indcrop.2023.117046.
[29] Z. Lou, Q. Wang, W. Sun, Y. Zhao, X. Wang, X. Liu, Y. Li, Bamboo flattening technique: a literature and patent review, European Journal of Wood and Wood Products 79 (2021) 1035–1048, https://doi.org/10.1007/s00107-021-01722-1.
[30] Z. Lou, Z. Zheng, N. Yan, X. Jiang, X. Zhang, S. Chen, R. Xu, C. Liu, L. Xu, Modification and application of bamboo-based materials: a review—Part II: application of bamboo-based materials, Forests 14 (2023) 2266, https://doi.org/10.3390/f14112266.
[31] E. Schmidt, M. Riggio, Monitoring moisture performance of cross-laminated timber building elements during construction, Buildings 9 (2019), https://doi.org/10.3390/BUILDINGS9060144.
[32] M.S. Austigard, J. Mattsson, Fungal damages in Norwegian massive timber elements–a case study, Wood Mater. Sci. Eng. 15 (2020) 326–334, https://doi.org/10.1080/17480272.2020.1801835.
[33] J. Niklewski, M. Fredriksson, The effects of joints on the moisture behaviour of rain exposed wood: a numerical study with experimental validation, Wood Mater. Sci. Eng. 16 (2021) 1–11, https://doi.org/10.1080/17480272.2019.1600163.
[34] L. Yermán, L.M. Ottenhaus, C. Montoya, J.J. Morrell, Effect of repeated wetting and drying on withdrawal capacity and corrosion of nails in treated and untreated timber, Construct. Build. Mater. 284 (2021), https://doi.org/10.1016/j.conbuildmat.2021.122878.
[35] A. Sinha, K.E. Udele, J. Cappellazzi, J.J. Morrell, A method to characterize biological degradation of mass timber connections, Wood Fiber Sci. 52 (2020) 419–430, https://doi.org/10.22382/wfs-2020-040.
[36] C. Larsson, O. Abdeljaber, T.K. Bader, M. Dorn, Modal analysis and finite element model updating of a timber-concrete hyblrid building, in: J. Kunecký, H. Hasníková (Eds.), SHATIS 2022: 6th International Conference on Structural Health Assessment of Timber Structures, Prague, 2022, pp. 193–199.
[37] A. Aloisio, D.P. Pasca, B. Kurent, M.M. Rosso, Y. De Santis, R. Tomasi, One-Year Dynamic Monitoring of an Eight Story CLT Building, 2024, pp. 712–719, https://doi.org/10.1007/978-3-031-61421-7_69.
[38] C. Larsson, O. Abdeljaber, M. Dorn, Dynamic evaluation of a nine-storey timber-concrete hybrid building during construction, Eng. Struct. 289 (2023) 116344, https://doi.org/10.1016/j.engstruct.2023.116344.
[39] T. Scheffer, A climate index for estimating potential for decay in wood structures above ground, For. Prod. J. 21 (1971) 25–31.
[40] R.W. Berry, Remedial Treatment of Wood Rot and Insect Attack in Buildings, Building Research Establishment, Watford, 1994.
[41] B. Goodell, 5 Fungi Involved in the Biodeterioration and Bioconversion of Lignocellulose Substrates, 2020.
[42] E.C. Setliff, Wood decay hazard in Canada based on Scheffer's climate index formula, For. Chron. (1986) 456–459.
[43] M. Hasegawa, Relationships between wood protection and climate indexes, Mokuzai Hozon 22 (1996) 2–9.
[44] C.H. Wang, R.H. Leicester, M.N. Nguyen, Decay above Ground, Manual No 4, CSIRO Sustainable Ecosystems, Urban Systems Program: Highett, 2008.
[45] K.R. Lisø, H.O. Hygen, T. Kvande, J.V. Thue, Decay potential in wood structures using climate data, Build. Res. Inf. 34 (2006) 546–551, https://doi.org/10.1080/09613210600736248.
[46] P.I. Morris, S. McFarling, J. Wang, A new decay hazard map for North America using the Scheffer Index, in: IRG Americas Regional Meeting, Playa Flamingo, 2008.
[47] C. Brischke, E. Hansson, E. Frühwald, D. Kavurmaci, S. Thelandersson, Decay hazard mapping for Europe, in: IRG Annual Meeting, Queenstown, 2011.
[48] EN 335, Durability of Wood and Wood-Based Products. Use Classes: Definitions, Application to Solid Wood and Wood-based Products, European Committee for Standardization, Brussels, 2013.
[49] Samuel V. Glass, Samuel L. Zelinka, Moisture relations and physical properties of wood, in: Wood Handbook – Wood as an Engineered Material, Forest Products Laboratory, Madison, 2021.
[50] K. Kalbe, V. Kukk, T. Kalamees, Identification and improvement of critical joints in CLT construction without weather protection. https://doi.org/10.1051/e3sconf/2020172, 2020.
[51] G.C. Rodrigues, R.P. Braga, Evaluation of nasa power reanalysis products to estimate daily weather variables in a hot summer mediterranean climate, Agronomy 11 (2021), https://doi.org/10.3390/agronomy11061207.
[52] H. Kadhim Tayyeh, R. Mohammed, Analysis of NASA POWER reanalysis products to predict temperature and precipitation in Euphrates River basin, J. Hydrol. (Amst.) 619 (2023), https://doi.org/10.1016/j.jhydrol.2023.129327.
[53] Y.T. Dile, R. Srinivasan, Evaluation of CFSR climate data for hydrologic prediction in data-scarce watersheds: an application in the Blue Nile River Basin, JAWRA Journal of the American Water Resources Association 50 (2014) 1226–1241, https://doi.org/10.1111/jawr.12182.
[54] S. Chen, T.Y. Gan, X. Tan, D. Shao, J. Zhu, Assessment of CFSR, ERA-Interim, JRA-55, MERRA-2, NCEP-2 reanalysis data for drought analysis over China, Clim. Dynam. 53 (2019) 737–757, https://doi.org/10.1007/s00382-018-04611-1.
[55] J.E. Nash, J.V. Sutcliffe, River flow forecasting through conceptual models part I — a discussion of principles, J. Hydrol. (Amst.) 10 (1970) 282–290, https://doi.org/10.1016/0022-1694(70)90255-6.
[56] C.J. Willmott, K. Matsuura, On the use of dimensioned measures of error to evaluate the performance of spatial interpolators, Int. J. Geogr. Inf. Sci. 20 (2006) 89–102, https://doi.org/10.1080/13658810500286976.
[57] D.R. Legates, G.J. McCabe, Evaluating the use of "goodness-of-fit" Measures in hydrologic and hydroclimatic model validation, Water Resour. Res. 35 (1999) 233–241, https://doi.org/10.1029/1998WR900018.

[58] M. Verbist, L. Nunes, D. Jones, J.M. Branco, Service life design of timber structures, in: Long-Term Performance and Durability of Masonry Structures, Elsevier, 2019, pp. 311–336, https://doi.org/10.1016/B978-0-08-102110-1.00011-X.
[59] E.J. Baas, M. Riggio, A.R. Barbosa, A methodological approach for structural health monitoring of mass-timber buildings under construction, Construct. Build. Mater. 268 (2021), https://doi.org/10.1016/j.conbuildmat.2020.121153.
[60] C. Brischke, V. Selter, Mapping the decay hazard of wooden structures in topographically divergent regions, Forests 11 (2020), https://doi.org/10.3390/F11050510.
[61] J. Bai, X. Chen, A. Dobermann, H. Yang, K.G. Cassman, F. Zhang, Evaluation of NASA satellite- and model-derived weather data for simulation of maize yield potential in China, Agron. J. 102 (2010) 9–16, https://doi.org/10.2134/agronj2009.0085.
[62] L.A. Monteiro, P.C. Sentelhas, G.U. Pedra, Assessment of NASA/POWER satellite-based weather system for Brazilian conditions and its impact on sugarcane yield simulation, Int. J. Climatol. 38 (2018) 1571–1581, https://doi.org/10.1002/joc.5282.
[63] M.R. Al-Kilani, M. Rahbeh, J. Al-Bakri, T. Tadesse, C. Knutson, Evaluation of remotely sensed precipitation estimates from the NASA POWER project for drought detection over Jordan, Earth Systems and Environment 5 (2021) 561–573, https://doi.org/10.1007/s41748-021-00245-2.
[64] Y. Kheyruri, A. Sharafati, Spatiotemporal assessment of the NASA POWER satellite precipitation product over different regions of Iran, Pure Appl. Geophys. 179 (2022) 3427–3439, https://doi.org/10.1007/s00024-022-03133-6.
[65] M. Shirmohammadi, A. Faircloth, Effect of alternate drying techniques on cross-laminated timber after exposure to free-water wetting, Forests 14 (2023), https://doi.org/10.3390/f14051007.
[66] J. Wang, Guide for On-Site Moisture Management of Wood Construction, FPInnovations, 2016.
[67] C. Brischke, S. Thelandersson, Modelling the outdoor performance of wood products – a review on existing approaches, Construct. Build. Mater. 66 (2014) 384–397, https://doi.org/10.1016/j.conbuildmat.2014.05.087.